A Relaxation Model for Numerical Approximations of the Multidimensional Pressureless Gas Dynamics System

SungKi Jung[§], and R. S. Myong*[,†]

§Centro de Engenharia, Modelagem e Ciências Sociais Aplicadas, Universidade Federal do ABC, Santo André, São Paulo, 09210-580, Brazil

sungki.jung@ufabc.edu.br

*School of Mechanical and Aerospace Engineering, Gyeongsang National University, Jinju, Gyeongnam, 52828, South Korea

[†] Research Center for Aircraft Core Technology, Gyeongsang National University, Jinju, Gyeongnam 52828, South Korea

Corresponding author*: myong@gnu.ac.kr*

Abstract

Relaxation models for the pressureless gas dynamics (PGD) equations attempt to satisfy the strictly hyperbolic conservation law in order to employ the well-posed approximated Riemann solvers. In this study, a new type of relaxation model is proposed to resolve two shortcomings of the existing relaxation models: the constant propagation speed of sound, and the collapse of delta shock waves in multidimensional problems. The proposed model seeks a strictly hyperbolic system of equations without any special consideration for the proper values of the propagation speed of sound. Numerical tests showed that the proposed model can accurately describe the behavior of the PGD equations, in particular, the occurrence of delta shock waves and vacuum states in a multidimensional problem.

Keywords: Pressureless gas dynamics equations, relaxation model, multidimensional problem, delta shock, vacuum

2010 MSC: 35L65, 65M08, 76N15

1. Introduction

A wide variety of physical phenomena is governed by pressureless gas dynamics (PGD)-type mathematical models. An important class of problems of practical interest includes dispersed phase transport within a continuous fluid phase in multiphase combustion [1, 2], liquid water droplets in the atmosphere [3], and alumina particles in rocket engines [2], as well as cosmology [4]. These particle flows result in the zero pressure of gas dynamic equations. The resulting PGD equations are a time-dependent system of non-linear partial differential equations of the hyperbolic type. Their main features are occurrences of delta shock waves and vacuum states, which bring non-trivial numerical challenges.

In general, both the shock wave and vacuum are well captured using existing Godunov-type upwind schemes [5]. These schemes, however, have been developed for the strictly hyperbolic conservation laws [6], and consequently they may not be carried over to the non-strictly hyperbolic conservation law case, due to lack of a distinct eigensystem [7, 8]. This presents a serious numerical difficulty for adopting the well-posed Godunov-type upwind schemes in the following PGD equations,

$$\begin{aligned} &\rho_t + (\rho u)_x = 0, \\ &(\rho u)_t + (\rho u^2)_x = 0, \end{aligned} \tag{1.1}$$

where, $t > 0$, $x \in \mathbb{R}$, and $\rho(x, t) \geq 0$ and $u(x, t)$ are in $\mathbb{R}$. Here, ρ and u denote the density and velocity of the gas or particle, respectively. The system of equations (1.1) represents the conservation of mass and momentum in the absence of pressure and has a non-diagonalizable Jacobian matrix with degenerate eigenvalues, $\mathbf{\Lambda}=[\lambda_1, \lambda_2]^T=[u, u]^T$. In order to derive the single-valued weak solutions to these equations, special treatments, like relaxation models, may be essential to circumvent the numerical difficulty associated with degenerate eigenvalues. Specifically, system (1.1) is modified as follows;

$$\begin{aligned} &\rho_t + (\rho u)_x = 0, \\ &(\rho u)_t + (\rho u^2 + \mathbf{A})_x = 0, \end{aligned} \tag{1.2}$$

where $\mathbf{A}=f(c, \rho)$ is an artificial term multiplied by a very small value of propagation speed of sound, $c \rightarrow 0$.

Most of the previous studies on relaxation models have focused on the isothermal and isentropic Euler equations. A state variable model and perturbation-based numerical scheme have been also studied with a small value of c. Table 1 presents several types of relaxation models for the PGD equations. Interestingly, all the models rely on a time-independent globally constant property of c, except for the model of Berthon *et al*. [7].

Table 1. Literature review on relaxation models for the PGD equations

Authors	Relaxation models	Remarks
Berthon *et al*. [7]	$\mathbf{A}=\Pi$, additional eq., $(\rho\Pi)_t+\nabla_{\mathbf{X}}\cdot(\rho\Pi u+c^2u)=0$	$c>0$
Chen *et al*. [8]	Isentropic ($\mathbf{A}=c\rho^{\gamma}$)	$\gamma>1$, c = const.
Bouchut *et al*. [9]	Isothermal ($\mathbf{A}=c^2\rho$)	$c=0.2$
Degond *et al*. [10]	$\mathbf{A}=\varepsilon P(\rho)$	$\varepsilon\rightarrow 0$, ε = const.
LeVeque [11]	Isothermal	$c\ll 1$, c = const.
Smith *et al*. [12]	Perturbation (ε)-based numerical scheme	$0<\varepsilon\ll 1$

Although these studies, based on one-dimensional tests, have demonstrated numerical accuracies in comparison with exact solutions of the PGD equations, there remain two unsolved issues; 1) the proper value of c in $\mathbf{A}$, and 2) the multidimensional effects of $\mathbf{A}$ beyond the simple one-dimensional case. For example, if using the depth positivity condition [14], the isothermal Euler equations may not provide the proper values (ranges) of c, because a logarithmic function of (A.6) derived by the generalized Riemann invariant has an infinite number at $\rho^*=0$, where ρ^* is a density in the region between the left and right waves identified by the eigensystem. In case of the isentropic Euler equations, c may be derived by minimum and maximum bounds with the ratio of specific heat γ. However, γ cannot be set up with a specified number due to the absence of pressure in the PGD equations. Hence, both isothermal and isentropic Euler equations cannot resolve issue 1), as described in the appendices.

In this study, a new type of relaxation model is proposed to derive the range of c and prevent the collapse of the delta shock wave in the multidimensional problem;

$$\begin{aligned}&\rho_t+(\rho u)_x=0,\\&(\rho u)_t+\left(\rho u^2+\mathbf{A}\right)_x=\mathbf{A}_x.\end{aligned}\tag{1.3}$$

The key idea is that, based on (1.3), minimum and maximum bounds of c are derived by invoking the positivity-preserving property, satisfying a positive density in the vacuum state, and the value of c is then presented as a time-dependent locally constant quantity. It turns out that the new relaxation model does not need any consideration for the proper value of c, effectively resolving issue 1). Also, (1.3) is mathematically equivalent to (1.1), so that it will not suffer the collapse of the delta shock wave in multidimensional space. The new relaxation model is derived by simply adding **A** into the left- and right-hand sides of the PGD equations as a splitting technique for purely numerical purposes. This splitting technique is motivated by the work of Myong *et al*. [13] in computational magnetohydrodynamics and by the work of Jung *et al*. [3] for Eulerian droplet equations in a dilute two-phase flow. Also, Menshov *et al*. [14] employed the splitting technique for calculation of the elastoplastic flows. The left-hand side in (1.3) naturally satisfies the strictly hyperbolic conservation law for which the well-posed approximate Riemann solvers can be employed, while the right-hand side can be treated as a source term.

In Section 2, the new relaxation model is described in detail, and then the minimum and maximum bounds of c are derived by invoking the depth positivity condition [15] and the generalized Riemann invariants across two opposite rarefaction waves. In Section 3, the HLLC approximated Riemann solver [16] for the numerical scheme of the new model is briefly reviewed. Wave-speed estimates are presented based on the generalized Riemann invariant across rarefaction waves and the Rankine-Hugoniot condition for the shock wave. Further, the treatment of the source term and associated finite volume formulation are briefly described. In Section 4, numerical tests of the one- and two-dimensional tests are presented to evaluate the performance of the new relaxation model.

2. A relaxation model for the multidimensional pressureless gas dynamics system

The relaxation models for the PGD equations can be expressed by a variety of hyperbolic systems of equations; for example, isothermal and isentropic Euler equations, in which c is assumed to be a very small constant. The shallow water equations can be also considered for a relaxation model of the PGD equations. The relaxation model of (1.3) can be rewritten with the help of the shallow water equations, as

$$\begin{aligned}
&\rho_t + \nabla_{\mathbf{x}} \cdot (\rho \mathbf{u}) = 0, \\
&(\rho \mathbf{u})_t + \nabla_{\mathbf{x}} \cdot \left(\rho \mathbf{u} \otimes \mathbf{u} + \frac{c^2 \rho^2}{\rho_a} \mathbf{I} \right) = \nabla_{\mathbf{x}} \cdot \left(\frac{c^2 \rho^2}{\rho_a} \mathbf{I} \right),
\end{aligned} \tag{2.1}$$

where, $t > 0$, $\mathbf{x} \in \mathbb{R}$, and $\rho(\mathbf{x}, t) \geq 0$ and $\mathbf{u}(\mathbf{x}, t)$ are in $\mathbb{R}$. Here, $\mathbf{u}$ denotes the velocity vector. $\mathbf{I}$ is an identity matrix, and ρ_a denotes an artificial density. Dividing ρ_a (=1) is introduced to be consistent with the physical unit in the momentum equation. Thus, ρ_a does not play any role in numerical simulations. $c^2\rho^2/\rho_a \mathbf{I}$ in (2.1) is in principle equivalent to the gravity term $0.5gh^2\mathbf{I}$ in the shallow water equations. Thus, the left-hand side of the model can be easily treated within the computational framework based on the approximate Riemann solver.

To study the bounds of c, the left-hand side of (2.1) can be rewritten in the one-dimensional non-conservative vector form,

$$\begin{aligned}
&\rho_t + u\rho_x + \rho u_x = 0, \\
&u_t + \frac{2c^2}{\rho_a} \rho_x + u u_x = 0,
\end{aligned} \tag{2.2}$$

and the Jacobian matrix of (2.2) becomes

$$\mathbf{F}(\mathbf{W}) = \begin{bmatrix} u & \rho \\ \dfrac{2c^2}{\rho_a} & u \end{bmatrix}, \tag{2.3}$$

where $\mathbf{W}=[\rho, u]^{\mathrm{T}}$. The eigenvalues and right eigenvectors of (2.3) are

$$\mathbf{\Lambda} = \left[u - a,\ u + a\right], \text{ and } \mathbf{R}_1 = \left[\rho,\ -a\right]^{\mathrm{T}},\ \mathbf{R}_2 = \left[\rho,\ a\right]^{\mathrm{T}}, \tag{2.4}$$

where $a = c\sqrt{2\rho/\rho_a}$.

In the Riemann problem, there are two wave families associated with the eigenvalues, λ_1 and λ_2 in (2.4). The two waves separate into three constant states denoted by $\mathbf{W}_L$, $\mathbf{W}_*$, and $\mathbf{W}_R$ from the left to the right.

The region between the left and right waves is defined as the star region. Then, the wave structure can be identified by the following conditions:

$$\rho_* > \rho_K : \text{shock wave},\ \rho_* \le \rho_K : \text{rarefaction wave}, \tag{2.5}$$

where a subscript *K* denotes the left and right states. By taking the generalized Riemann invariants across the left and right rarefaction waves into (2.3) and (2.4), we have

$$u_* = u_L - 2\left(a_* - a_L\right) \text{ for the left rarefaction wave,} \tag{2.6a}$$

$$u_* = u_R - 2\left(a_R - a_*\right) \text{ for the right rarefaction wave,} \tag{2.6b}$$

and, finally, we obtain the following relation,

$$u_R - u_L - 2\left(a_R + a_L\right) + 4a_* = 0. \tag{2.7}$$

Note the critical case of zero density in (2.7). The following condition at $\rho_* = 0$ must be fulfilled:

$$\left(\Delta u\right)_{crit} \equiv 2\left(a_R + a_L\right) \ge u_R - u_L. \tag{2.8}$$

(2.8) is called the *depth positivity condition* as proposed by Toro [15] and can be applied to the left-hand side of (2.1) and (2.2). Based on the depth positivity condition, the maximum and minimum bounds of *c* with a time-dependent locally constant property can be introduced in the following assumption and propositions.

Assumption 2.1. *Let us assume that the propagation speed of sound c is locally constant* $c = c(\mathbf{x},t) = c_L = c_R$ *and* $\rho_L > 0$ *and* $\rho_R > 0$ *as an initial value problem.*

Proposition 2.2. *The minimum bound of c has a time-dependent property identified by the left and right state variables,*

$$c_{\min} = \frac{1}{4}\frac{b\Delta u}{\bar{\rho}},$$

where, $\Delta u = u_R - u_L$, $\bar{\rho} = \frac{\sqrt{\rho_L} + \sqrt{\rho_R}}{2}$, $b = \sqrt{\frac{\rho_a}{2}}$.

Proof. $c_{\min}$ can be obtained by inserting $a = c\sqrt{2\rho/\rho_a}$ into (2.8),

$$2\left(c_R \sqrt{\frac{2\rho_R}{\rho_a}} + c_L \sqrt{\frac{2\rho_L}{\rho_a}} \right) \geq u_R - u_L,$$

and rearranging c using Assumption 2.1

$$c \geq \frac{1}{4} \frac{b\Delta u}{\bar{\rho}} \equiv c_{\min}.$$

$c_{\min}$ has a time-dependent property due to the left and right state variables, $c_{\min}=f(\mathrm{u}(\mathbf{x},t), \rho(\mathbf{x},t))$.

Proposition 2.3. *The maximum bound of c has a time-dependent property identified by the left and right state variables,*

$$c_{\max} = \frac{1}{4} \frac{b\Delta u}{\bar{\rho} - \rho_{\min}^{1/2}},$$

where $\rho_{\min} = \min(\rho_L, \rho_R)$.

Proof. The density ρ_* in the star region produced by two opposite rarefaction waves must be smaller than $\rho_{\min}$. Hence, (2.7) yields a simple relation among the state variables,

$$\rho_* = \left(\bar{\rho} - \frac{b\Delta u}{4c} \right)^2 < \rho_{\min},$$

and, after rearranging for c, we have

$$c < \frac{1}{4} \frac{b\Delta u}{\bar{\rho} - \rho_{\min}^{1/2}} \equiv c_{\max}.$$

The cases $\rho_{\min} = 0$, $c_{\max}=c_{\min}$ are included in Proposition 2.2. $c_{\max}$ also has a time-dependent property due to the left and right state variables, $c_{\max} = f(\mathrm{u}(\mathbf{x},t), \rho(\mathbf{x},t))$. Thus, the minimum and maximum bounds of

c, while locally constant, contain a time-dependent property. The wave speed estimates can be derived using Proposition 2.2 and 2.3.

3. Numerical scheme

The finite volume method with the Godunov-type upwind scheme is employed as a computational framework for the relaxation model. For the sake of simplicity, let us consider a one-dimensional x-split conservative vector form of (2.1),

$$\mathbf{U}_t + \mathbf{F}(\mathbf{U})_x = \mathbf{S}(\mathbf{U})_x, \tag{3.1}$$

and $\mathbf{U}=[\rho, \rho u, \rho\psi]^{\mathrm{T}}$, $\mathbf{F}(\mathbf{U})=[\rho u, \rho u^2+A, \rho u\psi]^{\mathrm{T}}$, $\mathbf{S}(\mathbf{U})=[0, A, 0]^{\mathrm{T}}$, where $A=c^2\rho^2/\rho_a$. A tangential velocity component ψ represents the concentration of a pollutant or other passive scalar. An integral form of (3.1) discretized on intervals $I_i=[x_{i-1/2}, x_{i+1/2}]$ becomes

$$\frac{\partial}{\partial t}\int_{x_{i-1/2}}^{x_{i+1/2}} \mathbf{U}(x,t)\,dx + \mathbf{F}\left(\mathbf{U}(x_{i+1/2},t)\right) - \mathbf{F}\left(\mathbf{U}(x_{i-1/2},t)\right) = \mathbf{S}\left(\mathbf{U}(x_{i+1/2},t)\right) - \mathbf{S}\left(\mathbf{U}(x_{i-1/2},t)\right). \tag{3.2}$$

When the cell average of interval I_i is defined as $\mathbf{U}_i = \frac{1}{\Delta x_i}\int_{x_{i-1/2}}^{x_{i+1/2}} \mathbf{U}(x,t)\,dx$, where $\Delta x_i = x_{i+1/2} - x_{i-1/2}$, the explicit finite volume conservative formula in the interval I_i can be derived:

$$\frac{d\mathbf{U}_i(t)}{dt} + \frac{1}{\Delta x_i}\left(\mathbf{F}_{x_{i+1/2}} - \mathbf{F}_{x_{i-1/2}}\right) = \frac{1}{\Delta x_i}\left(\mathbf{S}_{x_{i+1/2}} - \mathbf{S}_{x_{i-1/2}}\right), \tag{3.3}$$

where $\mathbf{F}_{i+1/2} = \mathbf{F}(\mathbf{U}_{i+1/2})$, $\mathbf{S}_{i+1/2} = \mathbf{S}(\mathbf{U}_{i+1/2})$, and $\mathbf{U}_{i+1/2} = \mathbf{U}(x_{i+1/2},t)$. The numerical fluxes $\mathbf{F}_{i+1/2}$ and $\mathbf{S}_{i+1/2}$, and the associated wave speed estimates can be derived using the Godunov-type upwind scheme.

The relaxation models for solving the PGD equations involve a critical numerical issue, the positivity of density in a vacuum. Accordingly, the positivity-preserving property of numerical schemes becomes the key to accurately resolving the nonlinear wave regions. Einfelt *et al*. [17] introduced a class of numerical schemes that always preserved the positivity of density from physical data. They showed that the Harten–Lax–van Leer (HLL) scheme [18] can serve as a positivity-preserving scheme because the absolute values

of the maximal and minimal wave speeds satisfy certain stability bounds. On the basis of these findings, Toro *et al*. [16] developed the Harten–Lax–van Leer-Contact (HLLC) approximate Riemann solver, which restores the contact and shear waves to account for the influence of intermediate waves, $\lambda=u$ in the HLL scheme. In this study, the HLLC approximate Riemann solver is employed for the new relaxation model.

3.1. HLLC solver for the relaxation model

Let us recall the left-hand side of (3.1) for the general initial value problem,

$$\mathbf{U}_t + \mathbf{F}\left(\mathbf{U}\right)_x = 0_x, \text{ and } \mathbf{U}\left(x,0\right) = \begin{cases} \mathbf{U}_L & \text{if} \quad x < 0, \\ \mathbf{U}_R & \text{if} \quad x > 0. \end{cases} \tag{3.4}$$

The Godunov inter-cell numerical flux $\mathbf{F}_{x_{i+1/2}}$ appearing in the explicit finite volume formulation can be derived for the HLLC solver as

$$\mathbf{F}_{i+1/2} = \begin{cases} \mathbf{F}_L & \text{if} \quad 0 \le S_L, \\ \mathbf{F}_{*L} & \text{if} \quad S_L \le 0 \le S_*, \\ \mathbf{F}_{*R} & \text{if} \quad S_* \le 0 \le S_R, \\ \mathbf{F}_R & \text{if} \quad S_R \le 0, \end{cases} \tag{3.5}$$

where $\mathbf{F}_{*K} = \mathbf{F}_K + S_K\left(\mathbf{U}_{*K} - \mathbf{U}_K\right)$, and the states $\mathbf{U}_{*K}$ are given by $\mathbf{U}_{*K} = \rho_K\left(\frac{S_K - u_K}{S_K - S_*}\right)\left[1, S_*, \psi_K\right]^{\mathrm{T}}$. The middle wave S_* in (3.5) can be obtained by assuming $\rho_{*L}=\rho_{*R}$ in the exact Riemann solver,

$$S_* = \frac{S_L\rho_R\left(u_R - S_R\right) - S_R\rho_L\left(u_L - S_L\right)}{\rho_R\left(u_R - S_R\right) - \rho_L\left(u_L - S_L\right)}. \tag{3.6}$$

The third component of the flux in (3.1) can be expressed in terms of the first component, that is, $\mathbf{F}^3=\mathbf{F}^1\psi$. In fact, the relation of the third component is derived from the solutions of the exact Riemann problem using the generalized Riemann invariant, $v_{*L}\neq v_{*R}$ and the Rankine-Hugoniot conditions, $v_*=v_R$ and $v_*=v_L$. An expression for the third component based on the velocity in a star region is given as

$$\mathbf{F}^3_{i+1/2} = \begin{cases} \mathbf{F}^1_{i+1/2}\psi_L & \text{if} \quad u_* \geq 0, \\ \mathbf{F}^1_{i+1/2}\psi_R & \text{if} \quad u_* < 0, \end{cases} \tag{3.7}$$

where $u_* = \frac{u_L + u_R}{2} + \frac{c}{b}\left(\sqrt{\rho_L} - \sqrt{\rho_R}\right)$ from (2.6a) and (2.6b), and u_* is only for the third component of the flux, which changes across the middle wave. In summary, the wave speeds, S_L and S_R, are required to compute the numerical fluxes as a closed form in the HLLC solver.

3.2. Wave-speed estimates

Several possible choices for estimating the wave speeds are available in the Riemann problem: a simple estimate by the direct use of eigenvalues [19], the Roe average eigenvalues for the left and right non-linear waves [20], and the exact solutions based on the Rankine-Hugoniot conditions and eigenvalues [16]. In this study, the wave speeds were estimated by applying the Rankine-Hugoniot condition for shock wave and the eigenvalues for the rarefaction wave into (2.2)-(2.4) as

$$S_L = u_L - a_L q_L, \text{ and } S_R = u_R + a_R q_R, \tag{3.8a}$$

where,

$$q_K = \begin{cases} \sqrt{0.5\left(\rho_* + \rho_K\right)\rho_*} \Big/ \rho_K & \text{if} \quad \rho_* > \rho_K \\ 1 & \text{if} \quad \rho_* \leq \rho_K \end{cases}, \tag{3.8b}$$

and $a_K = c\sqrt{2\rho_K / \rho_a}$. ρ_* in (3.8b) is the same as the one derived in Proposition 2.3, $\rho_* = \left(\bar{\rho} - \frac{b\Delta u}{4c}\right)^2$.

In (3.8a) and (3.8b), c is still too ambiguous to apply in the closed form of the HLLC solver, even though the minimum and maximum bounds of c are known. We need to determine the value of c.

Corollary 3.1. *c must avoid a singularity in the case that $\rho_L = \rho_R$ and be placed between $c_{\min}$ and $c_{\max}$*

$$c_{\min} = \frac{1}{4}\frac{b\Delta u}{\bar{\rho}} \leq c \equiv \frac{1}{4}\frac{b\Delta u}{\bar{\rho} - \frac{1}{2}\rho_{\min}^{1/2}} < c_{\max} = \frac{1}{4}\frac{b\Delta u}{\bar{\rho} - \rho_{\min}^{1/2}}.$$

3.3. Treatment of source term

The source term in (3.1) can be treated numerically using a splitting scheme [21]. The attraction of the splitting scheme is the simplicity and freedom available in choosing the numerical operators. The splitting scheme relies on solving the following two initial value problems,

$$\left.\begin{aligned}\mathbf{U}_t+\mathbf{F}\left(\mathbf{U}\right)_x=0,\\ \mathbf{U}\left(x,t^n\right)=\mathbf{U}^n,\end{aligned}\right\}\xrightarrow{\Delta t}\mathbf{U}^{adv},\ \text{and}\ \mathbf{U}_t=\mathbf{S}\left(\mathbf{U}^{adv}\right)_x\xrightarrow{\Delta t}\mathbf{U}^{n+1}, \tag{3.9}$$

where $\mathbf{U}^{adv}$ is regarded as a predicted solution. Then, (3.9) can be summarized to

$$\mathbf{U}_i^{n+1}=\mathbf{U}_i^n-\frac{\Delta t}{\Delta x}\left(\mathbf{F}_{i+1/2}-\mathbf{F}_{i-1/2}\right)+\frac{\Delta t}{\Delta x}\left(\mathbf{S}_{i+1/2}-\mathbf{S}_{i-1/2}\right), \tag{3.10}$$

where $\mathbf{F}_{i+1/2}=\mathbf{F}\left(\mathbf{U}_{i+1/2}^n\right)$ and $\mathbf{S}_{i+1/2}=\mathbf{S}\left(\mathbf{U}_{i+1/2}^{adv}\right)$. The source term can be treated by the HLLC solver,

$$\mathbf{S}_{i+1/2}=\begin{cases}\mathbf{S}_L & \text{if} \quad 0\le S_L,\\ \mathbf{S}_{*L} & \text{if} \quad S_L\le 0\le S_*,\\ \mathbf{S}_{*R} & \text{if} \quad S_*\le 0\le S_R,\\ \mathbf{S}_R & \text{if} \quad S_R\le 0,\end{cases} \tag{3.11}$$

where $\mathbf{S}_K=\left[0,\left(c\rho_K^{adv}\right)^2\Big/\rho_a,0\right]^{\mathrm{T}}$ and $\mathbf{S}_{*K}=\left[0,\left(c\rho_{*K}^{adv}\right)^2\Big/\rho_a,0\right]^{\mathrm{T}}$, and ρ_{*K}^{adv} is given by $\mathbf{U}_{*K}$ of (3.5).

3.4. Temporal discretization

(3.10) can be rewritten as

$$\mathbf{U}_i^{n+1}=\mathbf{U}_i^n-\lambda\left(\mathbf{Q}_{i+1/2}-\mathbf{Q}_{i-1/2}\right), \tag{3.12}$$

where $\mathbf{Q}_{i\pm1/2}=\mathbf{F}_{i\pm1/2}-\mathbf{S}_{i\pm1/2}$, $\lambda=\frac{\Delta t}{\Delta x}$, and $\Delta t=\dfrac{\mathrm{CFL}\cdot\Delta x}{\left(|u|+a\right)_{\max}}$. The following strong stability preserving (SSP) third-order Runge-Kutta time discretization [22] is used:

$$
\begin{aligned}
&\mathbf{U}^{(n+1/3)} = \mathbf{U}^n + \Delta t \mathbf{R}\left(\mathbf{U}^n\right), \\
&\mathbf{U}^{(n+2/3)} = \frac{3}{4}\mathbf{U}^n + \frac{1}{4}\mathbf{U}^{(n+1/3)} + \frac{1}{4}\Delta t \mathbf{R}\left(\mathbf{U}^{(n+1/3)}\right), \\
&\mathbf{U}^{n+1} = \frac{1}{3}\mathbf{U}^n + \frac{2}{3}\mathbf{U}^{(n+2/3)} + \frac{2}{3}\Delta t \mathbf{R}\left(\mathbf{U}^{(n+2/3)}\right).
\end{aligned} \tag{3.13}
$$

4. Numerical tests

We consider two numerical test cases: a typical one-dimensional test case studied by [7, 9, 11] for the PGD equations and a two-dimensional test case where two clouds collide. A special emphasis is placed on the propagation speed of sound c and the collapse of the delta shock wave in the two-dimensional problem. For numerical computations, the MUSCL-type second-order scheme [23] with Van Albada's limiter [24] is employed. The rotational invariance is applied to the relaxation model in the two-dimensional finite volume formulation. All the computations are carried out with $\mathbf{A} = c^2\rho^2/\rho_a\mathbf{I}$, $\rho_a = 1.0, \Delta x = \Delta y = 0.01$. The numerical solutions of (1.3) (with Corollary 3.1) and (1.2) (with constant c values) are compared with the exact solutions of (1.1).

4.1. 1-D test

This test is designed to create a vacuum and a mass accumulation. The initial conditions and the corresponding exact solutions at the time t=0.5 are

$$
\left(\rho_0,\, u_0\right) = \begin{cases} \left(0.5, -0.5\right) & \text{if} \quad x < -0.5, \\ \left(0.5, 0.4\right) & \text{if} \quad -0.5 < x < 0, \\ \left(0.5, 0.4 - x\right) & \text{if} \quad 0 < x < 0.8, \\ \left(0.5, -0.4\right) & \text{if} \quad x > 0.8, \end{cases}
$$

$$
\left(\rho_{0.5},\, u_{0.5}\right) = \begin{cases} \left(0.5,\ -0.5\right) & \text{if} \quad x < -0.75, \\ \left(0,\ \text{undefined}\right) & \text{if} \quad -0.75 < x < -0.3, \\ \left(0.5,\ 0.4\right) & \text{if} \quad -0.3 < x < 0.2, \\ \left(1,\ \frac{0.4-x}{0.5}\right) & \text{if} \quad 0.2 < x < 0.6, \\ \left(0.5,\ -0.4\right) & \text{if} \quad x > 0.6, \end{cases} \tag{4.1}
$$

where $\rho_0 = \rho_0(x)$ and $u_0 = u_0(x)$. All of the numerical solutions capture the delta shock wave and guarantee the positivity of density in the vacuum state, as shown in Fig. 1. As c decreases, the numerical solutions of (1.2) become closer to the exact solutions. In the case of (1.2) with c=0.01, a small CFL number (CFL=0.01) was used to avoid a local peak in density and fluctuations in velocities around the middle of the vacuum state. In the case of (1.2) with $c \leq 0.001$, even when a smaller CFL number was used, the computation broke down due to the presence of local extrema with $\Delta t \to 0$. This observation indicates that the (1.2)-type relaxation models may need careful treatment for selecting values of c and associated CFL numbers. On the other hand, (1.3) with Corollary 3.1 produces more accurate solutions around delta shocks and vacuum states, and allows a relatively high CFL number in the computation. The local oscillations around the delta shock waves were also observed in the density profile. The fundamental reason of local oscillations around shock waves is the use of the second order scheme, similar to the one reported by Bouchut *et al*. [9]. The first order scheme does not show the local oscillations; however, the first order scheme shows a spike within the density at the sonic point [7, 9]. Hence, a stronger monotonicity-preserving high order scheme may be needed to reduce these local oscillations.

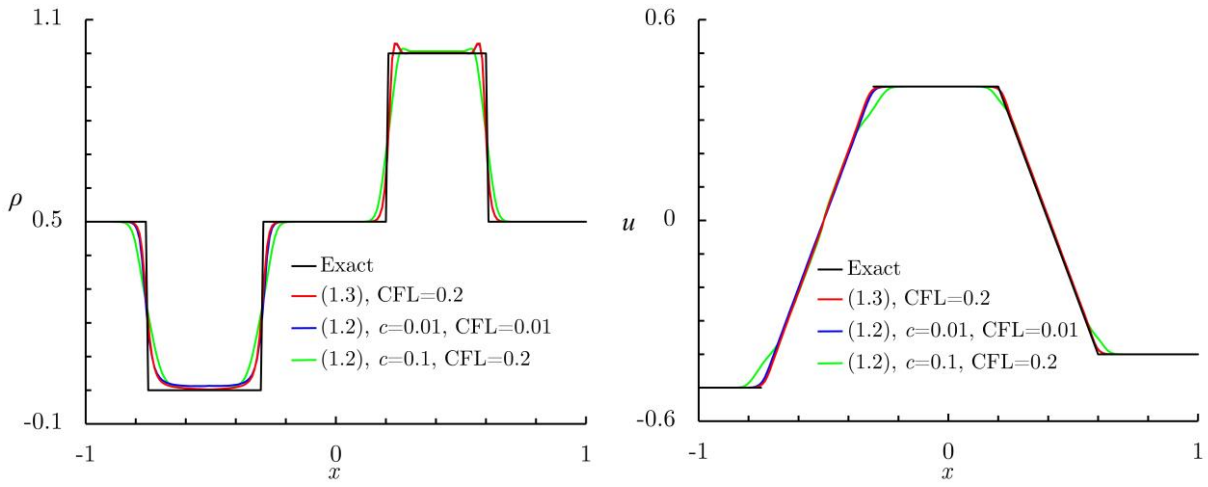

Fig 1. Exact solutions (—) of (1.1), numerical solutions of (1.2) with c=0.1 (—) and c=0.01 (—), and numerical solutions of (1.3) with Corollary 3.1 (—) on initial conditions in (4.1). Other parameters are taken to be $\mathbf{A}=\frac{c^2\rho^2}{\rho_a}\mathbf{I}$, ρ_a=1.0, $\triangle x$=0.01, and t=0.5.

4.2. 2-D test

A two-dimensional test is designed to compute the collapse of the delta shock and examine the effects of **A** in relaxation models in a multidimensional problem. The following initial conditions are considered,

$$(\rho_0, u_0, v_0) = \begin{cases} (1,\ 0.5,\ 0) & \text{if} \quad -0.3 < x < 0.2,\ -0.15 < y < 0.05, \\ (1,\ -0.5,\ 0) & \text{if} \quad 0.2 < x < 0.3,\ -0.05 < y < 0.15, \\ (0.1,\ 0,\ 0) & \text{otherwise.} \end{cases} \tag{4.2}$$

The solutions of the PGD equations with initial conditions of v=0, $u\neq0$ or u=0, $v\neq0$ do not affect any directional quantity due to the absence of pressure. That is, gases or particles do not change their directions and move their own way. If a small value of c in the relaxation models affects the entire domain in the PGD framework, careful attention must be paid to numerical computations based on these models, in particular, for the delta shock and vacuum state. For this purpose, two clouds with the same speed and density but opposite direction are considered. A part of each cloud entirely merges at $t\approx0.52$, and another part moves further on its own way after that.

In Fig. 2, the numerical solutions of (1.3) with Corollary 3.1 (CFL=0.2), (1.2) with c=0.01 (CFL=0.01), and (1.2) with c=0.1 (CFL=0.2) are compared. At t=0.2, (1.2) with c=0.1 starts to break, while the others retain their initial shape. At $t\approx0.52$, (1.2) with c=0.1 shows a delta shock at the center, but a moderate collapse already took place, indicated by the weaker delta shock. In the case of (1.2) with c=0.01, the clouds start to break around the upper and lower edges of the colliding part of the clouds.

At t=0.8, (1.3) with Corollary 3.1 shows a strong delta shock at the center and the non-colliding parts of clouds still keep their directions, indicating that the collapse of the delta shock did not occur in the multidimensional problem. In contrast, (1.2) with c=0.1 shows a large circulation as a direct result of the complete collapse of the delta shock. Also, (1.2) with c=0.01 shows a weak collapse at the interface between the colliding and non-colliding parts. Further, the computation of (1.2) with c=0.01 was not able to advance beyond t=0.8, due to the formation of local extrema with $\Delta t \to 0$.

Figure 3 shows densities and velocities at a section x=0 of the domain with time of t≈0.52 and t=0.8. The model (1.3) with Corollary 3.1 shows very stable density and velocity distributions without any fluctuations in the y direction. In particular, a maximum v velocity at the given time is very small, 1.0e-26. In contrast, (1.2) with c=0.1 and c=0.01 shows large fluctuations and amplifications in the v velocities increasing gradually with time. Further, (1.2) with c=0.01 shows that, unlike (1.3) with Corollary 3.1, the shock waves become weak at the interface between the colliding and non-colliding parts and non-uniformly distributed densities are observed in the colliding part, where the densities must have uniform distributions at the given conditions under the PGD system. Based on this observation, the (1.2)-type relaxation models may need careful treatment for the multidimensional PGD system, even when the 1-D test may provide accurate solutions.

(1.3), CFL=0.2

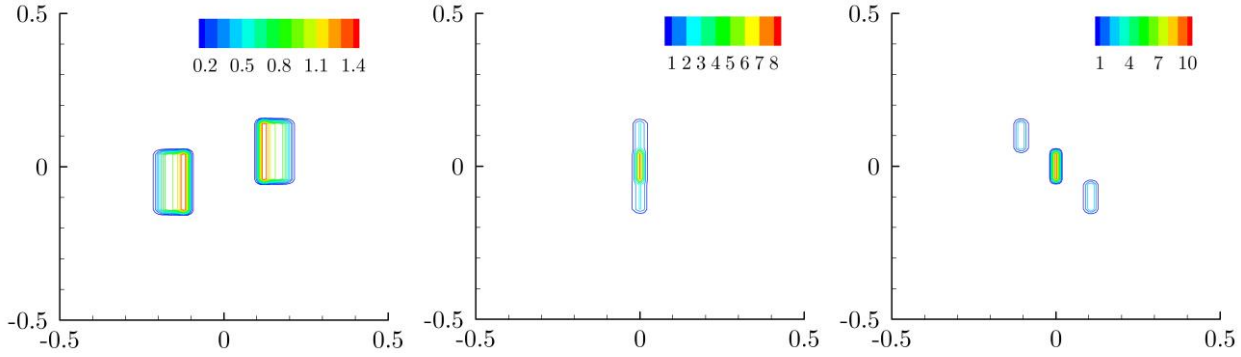

(1.2), c=0.01, CFL=0.01

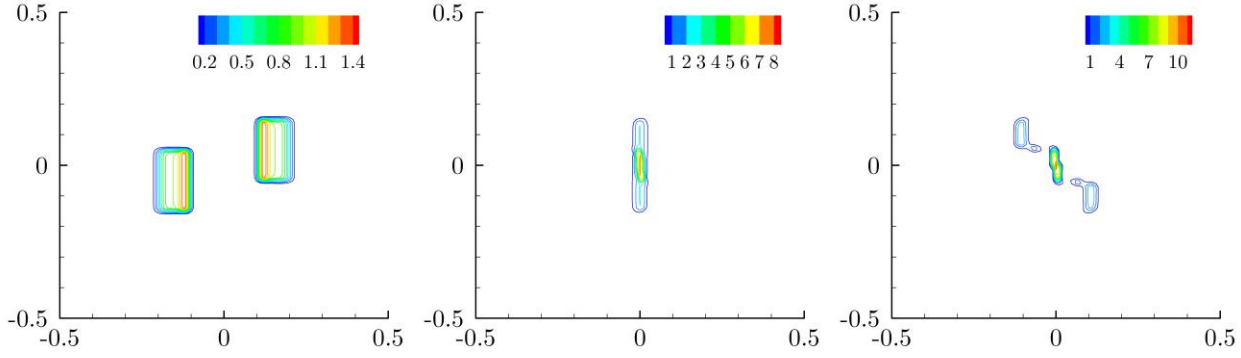

(1.2), c=0.1, CFL=0.2

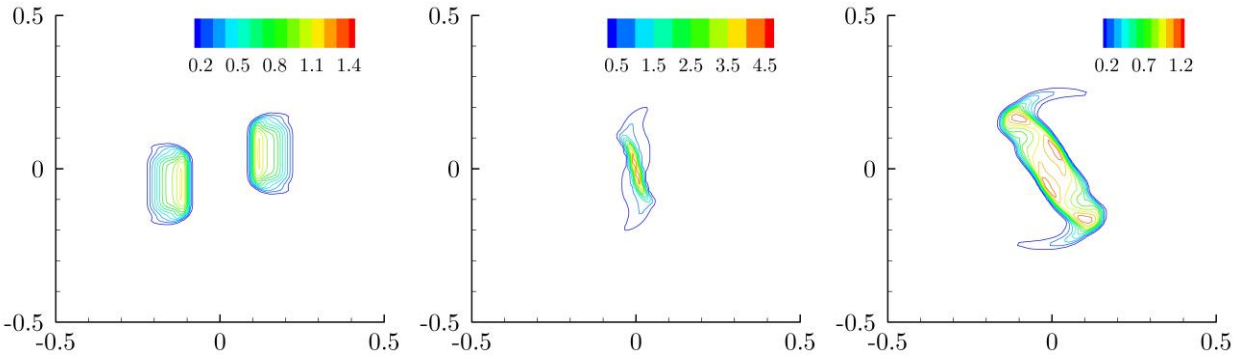

t=0.2 t≈0.52 t=0.8

Fig. 2. Density fields according to the relaxation models (upper: (1.3) with Corollary 3.1 and CFL=0.2, middle: (1.2) with c=0.01 and CFL=0.01, lower: (1.2) with c=0.1 and CFL=0.2) at various times (left: t=0.2, middle: t≈0.52, right: t=0.8) on initial conditions in (4.2). Other parameters are taken to be $\mathbf{A}=c^2\rho^2/\rho_a\mathbf{I}$, ρ_a=1.0, $\triangle x=\triangle y$=0.01.

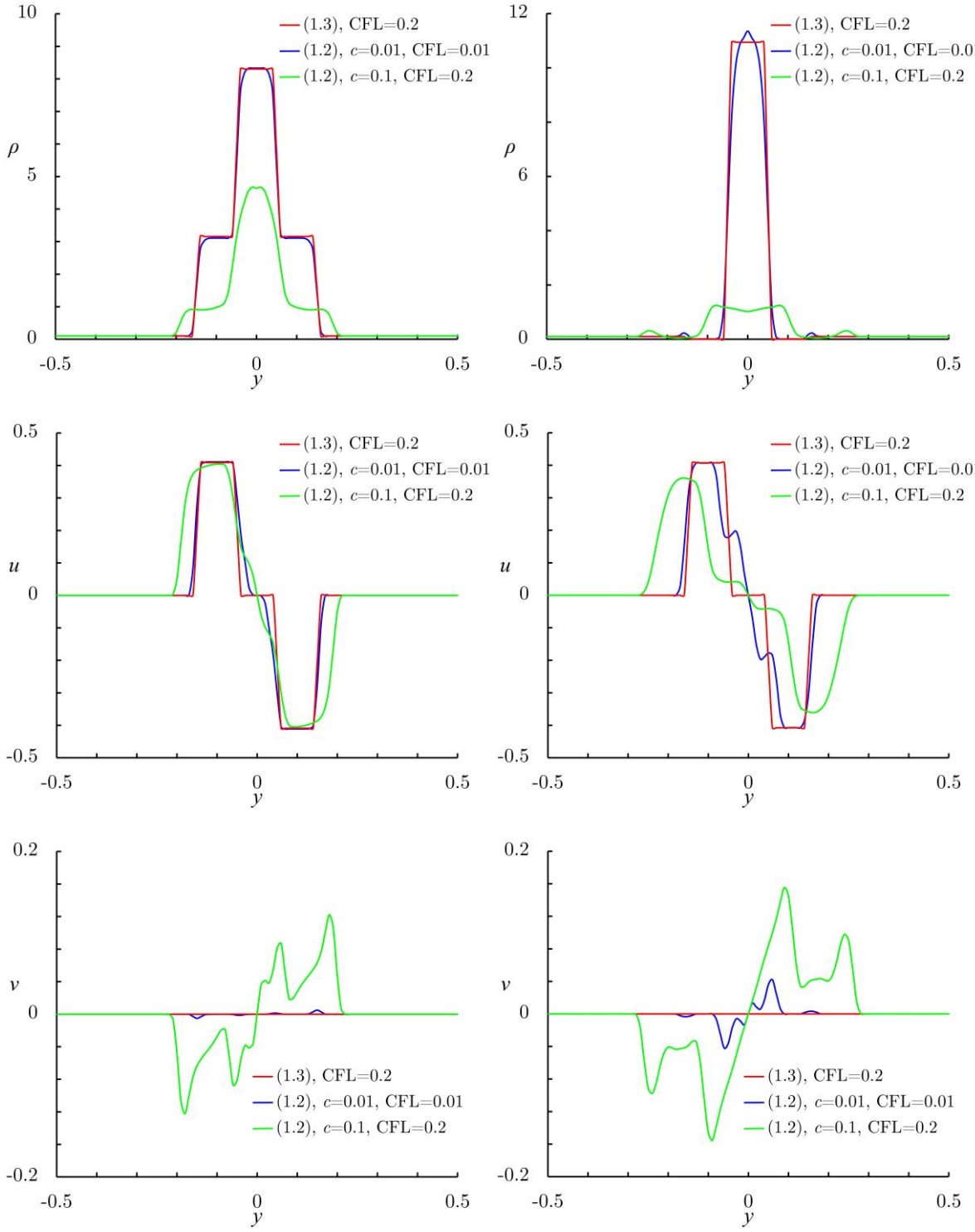

Fig. 3. Numerical solutions of (1.2) with c=0.1 (—) and c=0.01 (—), and numerical solutions of (1.3) with Corollary 3.1 (—) at a section x=0 and various times (left: $t\approx$0.52 and right: t=0.8) on initial conditions in (4.2). Other parameters are taken to be $\mathbf{A}=c^2\rho^2/\rho_a\mathbf{I}$, ρ_a=1.0, $\triangle x=\triangle y$=0.01.

5. Conclusions

The relaxation models for the PGD equations have a major advantage because they enable the use of the well-posed approximated Riemann solvers for delta shock and vacuum. Two tricky questions remained, however, in the existing relaxation models; how small the value of the propagation speed of sound should be to guarantee the numerical accuracy of the relaxation models, and how to prevent the collapse of the delta shock wave in multidimensional problems.

To solve these problems, we proposed a new relaxation model based on the idea of adding an artificial term to both sides of the multidimensional PGD equations and a propagation speed of sound with a time-dependent locally constant property. The numerical tests showed that the proposed model can accurately describe the behaviors of the PGD equations, in particular, the delta shock waves and vacuum states in a multidimensional problem. In the future, a monotonicity-preserving high order scheme for reducing the local oscillations around shock waves will be studied.

Acknowledgments

This work was supported by the National Research Foundation of Korea (NRF) Grant funded by the Ministry of Science and ICT (NRF-2017-R1A5A1015311), South Korea.

Appendix A: Uncertainty of a propagation speed of sound in the isothermal Euler equations

The isothermal Euler equations for (1.2)-type relaxation model are

$$\begin{aligned} &\rho_t + \nabla_{\mathbf{x}} \cdot (\rho \mathbf{u}) = 0, \\ &(\rho \mathbf{u})_t + \nabla_{\mathbf{x}} \cdot (\rho \mathbf{u} \otimes \mathbf{u} + c^2 \rho) = 0, \end{aligned} \tag{A.1}$$

where c is a positive constant propagation speed of sound. The Jacobian matrix of (A.1) in a conservative form becomes

$$\mathbf{F}(\mathbf{W}) = \begin{bmatrix} 0 & 1 \\ c^2 - u^2 & 2u \end{bmatrix}, \tag{A.2}$$

where $\mathbf{W}=[\rho, \rho u]^{\mathrm{T}}$. The eigenvalues and right eigenvectors of (A.2) are

$$\mathbf{\Lambda} = [u-c,\ u+c], \text{ and } \mathbf{R}_1 = [1,\ u-a]^{\mathrm{T}},\ \mathbf{R}_2 = [1,\ u+a]^{\mathrm{T}}. \tag{A.3}$$

Then, the generalized Riemann invariants across the left and right rarefaction waves into (A.3) give

$$u_* = u_L - c(\ln \rho_* - \ln \rho_L) \text{ for the left rarefaction wave,} \tag{A.4a}$$

$$u_* = u_R - c(\ln \rho_R - \ln \rho_*) \text{ for the right rarefaction wave,} \tag{A.4b}$$

where ρ_R, ρ_L, and ρ_* must be positive. Then, we obtain the following relation,

$$u_R - u_L - c(\ln \rho_R + \ln \rho_L) + 2c \ln \rho_* = 0, \tag{A.5}$$

and, after rearranging for ρ_*, we have

$$\rho_* = \left(\frac{\rho_R \rho_L}{e^{\Delta u/c}} \right)^{0.5} \geq 0, \tag{A.6}$$

where $\triangle u = u_R - u_L$. Note the critical case of $\rho_* = 0$ in (A.6). A propagation speed of sound c satisfying the depth positivity condition at $\rho_* = 0$ remains uncertain due to a logarithmic function of ρ_* in the isothermal Euler equations.

Appendix B: Uncertainty of a propagation speed of sound in isentropic Euler equations

The isentropic Euler equations for (1.2)-type relaxation model are

$$\begin{aligned} &\rho_t + \nabla_{\mathbf{x}} \cdot (\rho \mathbf{u}) = 0, \\ &(\rho \mathbf{u})_t + \nabla_{\mathbf{x}} \cdot (\rho \mathbf{u} \otimes \mathbf{u} + c\rho^{\gamma}) = 0, \end{aligned} \tag{B.1}$$

where c is a positive constant propagation speed of sound and γ is the ratio of specific heat. The Jacobian matrix of (B.1) in a conservative form becomes

$$\mathbf{F}(\mathbf{W}) = \begin{bmatrix} 0 & 1 \\ a^2 - u^2 & 2u \end{bmatrix}, \tag{B.2}$$

where $\mathbf{W}=[\rho, \rho u]^{\mathrm{T}}$. and $a^2=c\gamma\rho^{\gamma-1}$. The eigenvalues and right eigenvectors of (B.2) are

$$\mathbf{\Lambda} = \left[u-a,\ u+a\right], \text{ and } \mathbf{R}_1 = \left[1,\ u-a\right]^{\mathrm{T}},\ \mathbf{R}_2 = \left[1,\ u+a\right]^{\mathrm{T}}. \tag{B.3}$$

Then, the generalized Riemann invariants across the left and right rarefaction waves into (B.3) give

$$u_* = u_L - \frac{2}{\gamma-1}\left(a_* - a_L\right) \text{ for the left rarefaction wave,} \tag{B.4a}$$

$$u_* = u_R - \frac{2}{\gamma-1}\left(a_R - a_*\right) \text{ for the right rarefaction wave,} \tag{B.4b}$$

and we then obtain the following relation,

$$u_R - u_L - \frac{2}{\gamma-1}\left(a_R + a_L\right) + \frac{4}{\gamma-1}a_* = 0. \tag{B.5}$$

Based on the depth positivity condition, the minimum bound of c in (B.5) can be derived using the assumption 2.1. and proposition 2.2. That is,

$$c_{\min} \equiv \frac{b^2}{\gamma}\left(\frac{\Delta u}{\rho_L^b + \rho_R^b}\right)^2 \le c, \tag{B.6}$$

where $b=\frac{\gamma-1}{2}$ and $\triangle u=u_R-u_L$. Similarly, the maximum bound of c can be derived using the assumption 2.1. and proposition 2.3. That is,

$$c < \frac{b^2}{4\gamma}\left(\frac{\Delta u}{0.5\left(\rho_L^b + \rho_R^b\right) - \rho_{\min}^b}\right)^2 \equiv c_{\max}, \tag{B.7}$$

where $\rho_{\min}=\min(\rho_L, \rho_R)$. After rearranging (B.6) and (B.7) for c, we have

$$\frac{b^2}{\gamma}\left(\frac{\Delta u}{\rho_L^b + \rho_R^b}\right)^2 \le c < \frac{b^2}{4\gamma}\left(\frac{\Delta u}{0.5\left(\rho_L^b + \rho_R^b\right) - \rho_{\min}^b}\right)^2. \tag{B.8}$$

The isentropic Euler equations can serve as a relaxation model for the PGD equations. However, the ratio of specific heat γ appearing in (B.8) cannot be set up due to the absence of pressure in the PGD equations. Additionally, any parameter for γ in (B.8) may be considered. However, it is still ambiguous, since (B.8) is invalid in three cases of γ (γ <0, γ=0, γ=1). Hence, a propagation speed of sound c also remains uncertain in the isentropic Euler equations.

References

[1] M. Boileau, C. Chalons, and M. Massot, Robust numerical coupling of pressure and pressureless gas dynamics equations for Eulerian spray DNS and LES, SIAM Journal on Scientific Computing, 37 (2015), pp. 79–102.
[2] S. Hank, R. Saurel, and O. Le Metayer, A hyperbolic Eulerian model for dilute two-phase suspensions, Journal of Modern Physics, 2 (2011), pp. 997–1011.
[3] S. K. Jung and R. S. Myong, A second-order positivity-preserving finite volume upwind scheme for air-mixed droplet flow in atmospheric icing, Computers and Fluids, 86 (2013), pp. 459–469.
[4] M. Vergassola, B. Dubrulle, U. Frisch, and A. Noullez, Burgers equation, devils staircases and the mass distribution for large-scale structures, Astronomy and Astrophysics, 289 (1994), pp. 325–356.
[5] P. Glaister, An efficient numerical scheme for the Euler equations, Computers and Mathematics with Applications, 27(8) (1994), pp. 91–100.
[6] A. Serezhkin, Mathematical modeling of wide-range compressible two-phase flows, Computers and Mathematics with Applications, 78(2) (2019), pp. 517–540.
[7] C. Berthon, M. Breub, and M. O. Titeux, A relaxation scheme for the approximation of the pressureless Euler equations, Numerical Methods for Partial Differential Equations, 22 (2006), pp. 484–505.
[8] G. Q. Chen and H. Liu, Formation of δ-shocks and vacuum states in the vanishing pressure limit of solutions to the Euler equations for isentropic fluids, SIAM Journal on Mathematical Analysis, 34 (2003), pp. 925–938.
[9] F. Bouchut, S. Jin, and X. Li, Numerical approximations of pressureless and isothermal gas dynamics, SIAM Journal on Numerical Analysis, 41 (2003), pp. 135–158.
[10] P. Degond, J. Hua, and L. Navoret, Numerical simulations of the Euler system with congestion constraint, Journal of Computational Physics, 230 (2011), pp. 8057–8088.
[11] R. J. LeVeque, The dynamics of pressureless dust clouds and delta waves, Journal of Hyperbolic Differential Equations, 1 (2004), pp. 315–327.
[12] T. A. Smith, D. J. Petty, and C. Pantano, A Roe-like numerical method for weakly hyperbolic systems of equations in conservation and non-conservation form, Journal of Computational Physics, 316 (2016), pp. 117–138.
[13] R. S. Myong and P. L. Roe, On Godunov-type schemes for magnetohydrodynamics. Part 1. A model system, Journal of Computational Physics, 147 (1998), pp. 545–567.
[14] I. Menshov, A. Mischenko, and A. Serezhkin, An Eulerian Godunov-type scheme for calculation of the elastic-plastic flow equations with moving grids, Mathematical Models and Computer Simulations, 6(2) (2014), pp. 127−141.
[15] E. F. Toro, Shock-Capturing Methods for Free-Surface Shallow Flows, John Wiley and Sons, Ltd., 2001.
[16] E. F. Toro, M. Spruce, and W. Speares, Restoration of the contact surface in the HLL-Riemann solver, Shock Waves, 4 (1994), pp. 25–34.

[17] B. Einfeldt, C. Munz, P. L. Roe, and B. J. Sjögreen, On Godunov-type methods near low densities, Journal of Computational Physics, 92 (1991), pp. 273–295.
[18] A. Harten, P. D. Lax, and B. van Leer, On upstream differencing and Godunov-type schemes for hyperbolic conservation laws, SIAM Review, 25 (1983), pp. 35–61.
[19] S. F. Davis, Simplified second-order Godunov-type methods, SIAM Journal on Scientific and Statistical Computing, 9 (1988), pp. 445–473.
[20] B. Einfeldt, On Godunov-type methods for gas dynamics, SIAM Journal on Numerical Analysis, 25 (1988), pp. 294–318.
[21] E. F. Toro, Riemann Solvers and Numerical Methods for Fluid Dynamics, A Practical Introduction, Springer Berlin Heidelberg, 2009.
[22] S. Gottlieb, D. Ketcheson, and C. W. Shu, High order strong stability preserving time discretizations, Journal of Scientific Computing, 38 (2009), pp. 251–289.
[23] B. van Leer, Towards the ultimate conservative difference scheme, V. a second-order sequel to Godunov's method, Journal of Computational Physics, 32 (1979), pp. 101–136.
[24] G. D. V. Albada, B. V. Leer, and W. W. Roberts, A comparative study of computational methods in cosmic gas dynamics, Astronomy and Astrophysics, 108 (1982), pp. 76–84.